Uniaxial Mechanical Characterization of Silicone and Porcine Muscle: Ogden Hyperelastic Modeling and Viscoelastic Comparison

Siyi Li

Department of Chemical, Paper, and Biomedical Engineering
Miami University

Abstract

This study examined the large-deformation mechanical behavior of silicone rubber and porcine skeletal muscle through uniaxial tensile and compressive testing to characterize nonlinear elasticity, viscoelastic relaxation, and the suitability of constitutive models. Three silicone strip specimens were subjected to high-rate uniaxial tension using a displacement-controlled protocol in which each strip was stretched at 400 mm/min from its initial 200-mm gauge length to a total extension of 200 mm, producing a stretch ratio of approximately $\lambda \approx 2$. The loading phase was immediately followed by a full unloading cycle, allowing observation of hysteresis and energy dissipation. In parallel, three cylindrical silicone specimens and three porcine muscle specimens were tested under unconfined compression. Each sample was compressed by 3.3 mm at a constant rate of 5 mm/min, after which the displacement was held for 120 seconds to measure stress relaxation. Engineering stress–strain curves were computed using measured forces and original specimen dimensions, and stress-time curves were extracted to quantify viscoelastic decay.

Silicone exhibited highly repeatable nonlinear elastic behavior across all tensile specimens, with pronounced hysteresis during the load–unload cycle and substantial relaxation during compression. Porcine muscle, in contrast, showed lower stiffness, stronger time-dependent decay, and larger variability between samples, consistent with structurally heterogeneous biological tissue. To model the nonlinear elastic response, the first loading segment of the tensile data was fitted to a four-term Ogden hyperelastic model, a widely used formulation for elastomeric and biological materials capable of capturing strain-stiffening behavior (Ogden, 1972). The fitted model parameters provided good agreement with the experimental tensile curves, demonstrating that silicone rubber behaves as a hyperelastic material under large stretch and validating the applicability of multi-term Ogden formulations for soft-tissue analogues. It is noted that the fitted exponents appear in near-identical pairs ($\alpha_1 \approx \alpha_3$, $\alpha_2 \approx \alpha_4$), suggesting the response is governed by two dominant deformation mechanisms; a two-term model may warrant investigation in future work.

Overall, the results highlight clear contrasts between the mechanical behavior of synthetic elastomers and biological tissue under tension and compression, while demonstrating the effectiveness of hyperelastic modeling in interpreting large-strain responses in soft materials.

1 Objectives

The objective of this laboratory study was to characterize the nonlinear, large-deformation mechanical behavior of soft biological and synthetic materials using uniaxial loading protocols and to express their responses in terms of continuum mechanical stress measures suitable for constitutive modeling. Unconfined compression tests were performed on cylindrical silicone rubber and porcine skeletal muscle specimens to quantify large-strain axial deformation, nonlinear stress–strain characteristics, and stress-relaxation kinetics under displacement-controlled loading. Each specimen was compressed by 3.3 mm at 5 mm/min, after which the deformation gradient F was held fixed for 120 s to isolate time-dependent relaxation governed by intrinsic viscoelasticity, fluid redistribution, and tissue microstructural reorganization.

Complementary tensile tests were conducted on silicone strips to probe their behavior under large principal stretch. Each strip was elongated from an initial gauge length of 200 mm to an additional 200 mm extension at 400 mm/min, generating principal stretches on the order of $\lambda_1 \approx 2$. Under the assumption of incompressibility ($\mathrm{J} = \det \mathrm{F} = 1$), the lateral stretches satisfied $\lambda_2 = \lambda_3 = \lambda_1^{-1/2}$, enabling analysis of the full principal stretch state. Tensile loading–unloading cycles were used to quantify strain stiffening, mechanical hysteresis, and energy dissipation typical of elastomeric solids.

A further objective was to transform raw force–displacement measurements into an appropriate stress measure for constitutive evaluation. Engineering stress–strain curves were computed using the undeformed sample geometry, where the engineering (first Piola–Kirchhoff) stress is defined as

$$P = \frac{F}{A_0},$$

where F is the axial force and A_0 is the undeformed cross-sectional area. This stress measure is directly accessible from the experiment and is the appropriate quantity to compare against hyperelastic model predictions under uniaxial loading.

The final objective was to determine whether the nonlinear elastic component of silicone's tensile response could be captured using an incompressible four-term Ogden hyperelastic energy density function,

$$W = \sum_{i=1}^{4} \frac{\mu_i}{\alpha_i}(\lambda_1^{\alpha_i} + \lambda_2^{\alpha_i} + \lambda_3^{\alpha_i} - 3),$$

and to identify the material parameters μ_i, α_i through nonlinear least-squares fitting of the first Piola–Kirchhoff stress data. This assessment enabled evaluation of the Ogden model's ability to represent strain stiffening and large-deformation elasticity in silicone rubber.

2 Methods

2.1 Specimen Preparation and Geometric Characterization

Cylindrical silicone rubber and porcine skeletal muscle specimens were prepared for unconfined compression testing, while silicone strip specimens were prepared for uniaxial

tension. The diameter and initial height of each cylindrical specimen were measured using a digital caliper, and the width, thickness, and initial gauge length of each tensile strip were recorded. The geometric measurements were used to compute reference cross-sectional areas and to define the undeformed configuration (A_0, L_0) required for engineering and continuum-mechanical stress calculations.

For tensile specimens, the initial gauge length was fixed at 200 mm, with width and thickness recorded for each strip. For compression specimens, diameters ranged from approximately 14–18.8 mm and initial heights from 15–23.4 mm, depending on the material. These linear dimensions defined the reference configuration from which deformation gradients and principal stretches were computed.

2.2 Mechanical Testing Protocol

All mechanical tests were performed using a displacement-controlled universal testing machine (TestResources SM-500-294/Instron 2519-105). Representative photographs of the experimental configurations are provided in Figure 12.

Uniaxial Tension (Silicone Only)

Three silicone strips were subjected to a cyclic load-unload protocol. Specimens were clamped with an initial gauge length of $L_0 = 200$ mm and stretched to a maximum extension of 200 mm ($\lambda = 2$) at a rate of 400 mm/min. The loading phase was immediately followed by unloading to the initial position to observe hysteresis. Note that no stress relaxation hold phase was applied during tensile testing.

Uniaxial Compression (Silicone and Muscle)

Compression tests were conducted on three silicone cylinders and three porcine muscle cylinders. Each specimen was compressed by 3.3 mm at a rate of 5 mm/min. Upon reaching maximum displacement, the crosshead position was held constant for 120 seconds to record the stress relaxation response. Force F and displacement d data were recorded continuously and converted to engineering stress ($P = F/A_0$) and stretch ratio ($\lambda = 1 + \Delta L/L_0$).

2.3 Constitutive Modeling

To characterize the large-deformation behavior of the silicone elastomer, the experimental data were fitted to the incompressible Ogden hyperelastic model. The strain energy density function W for an incompressible isotropic material is given by:

$$W(\lambda_1, \lambda_2, \lambda_3) = \sum_{i=1}^{N} \frac{\mu_i}{\alpha_i} (\lambda_1^{\alpha_i} + \lambda_2^{\alpha_i} + \lambda_3^{\alpha_i} - 3)$$

where μ_i are the shear moduli, α_i are dimensionless material constants, and N is the number of terms in the series.

For the case of uniaxial deformation (where $\lambda_1 = \lambda$ and $\lambda_2 = \lambda_3 = \lambda^{-1/2}$), the corresponding engineering stress P is derived as:

$$P = \frac{\partial W}{\partial \lambda} = \sum_{i=1}^{N} \mu_i \left(\lambda^{\alpha_i - 1} - \lambda^{-\frac{\alpha_i}{2} - 1} \right)$$

This quantity corresponds directly to the engineering stress measured experimentally, and all model fits in this work were performed using this stress measure.

For the tensile data (large deformation), a four-term approximation ($N = 4$) was employed to capture the strain-stiffening response. For compression data (small deformation), a simplified one-term model ($N = 1$) was sufficient. Model parameters were determined using a nonlinear least-squares optimization algorithm (Python, SciPy) to minimize the sum of squared errors (SSE) between the model prediction and experimental data.

Note on stress notation: Throughout this report, stress–strain figures display axis labels using σ; however, the plotted quantity in all cases is the first Piola–Kirchhoff (engineering) stress $P = F/A_0$, which is directly accessible from the experimental force and undeformed cross-sectional area.

3 Results

3.1 Uniaxial Tensile Response of Silicone

All three silicone strip specimens exhibited smooth, nonlinear elastic responses under uniaxial tension. The engineering stress–strain curves showed consistent repeatability across specimens, with only minor variation in initial compliance and peak stress. As axial stretch increased, the engineering stress rose monotonically, reflecting the characteristic strain-stiffening behavior of rubber-like, nearly incompressible materials.

During unloading, each specimen demonstrated pronounced hysteresis relative to the loading path, indicating mechanical energy dissipation associated with viscoelasticity in silicone elastomers. The overall shape of the curves is consistent with exponential-type constitutive behavior typically captured by Ogden or related hyperelastic formulations. The tensile stress–strain responses for the three specimens are shown in Figure 1.

3.2 Unconfined Compression Response of Silicone

The silicone cylinders subjected to unconfined compression exhibited smooth and repeatable nonlinear stress–strain behavior across all specimens. The initial response was compliant, followed by progressive stiffening as the axial engineering strain increased. This characteristic J-shaped curve reflects hyperelastic behavior typical of silicone elastomers, in which effective stiffness rises with increasing deformation.

Overall, the three specimens showed minimal sample-to-sample variability, indicating consistent material fabrication and uniform mechanical properties. The resulting engineering stress–strain curves are presented in Figure 2, demonstrating similar levels of initial compliance, curvature, and peak stress for all samples.

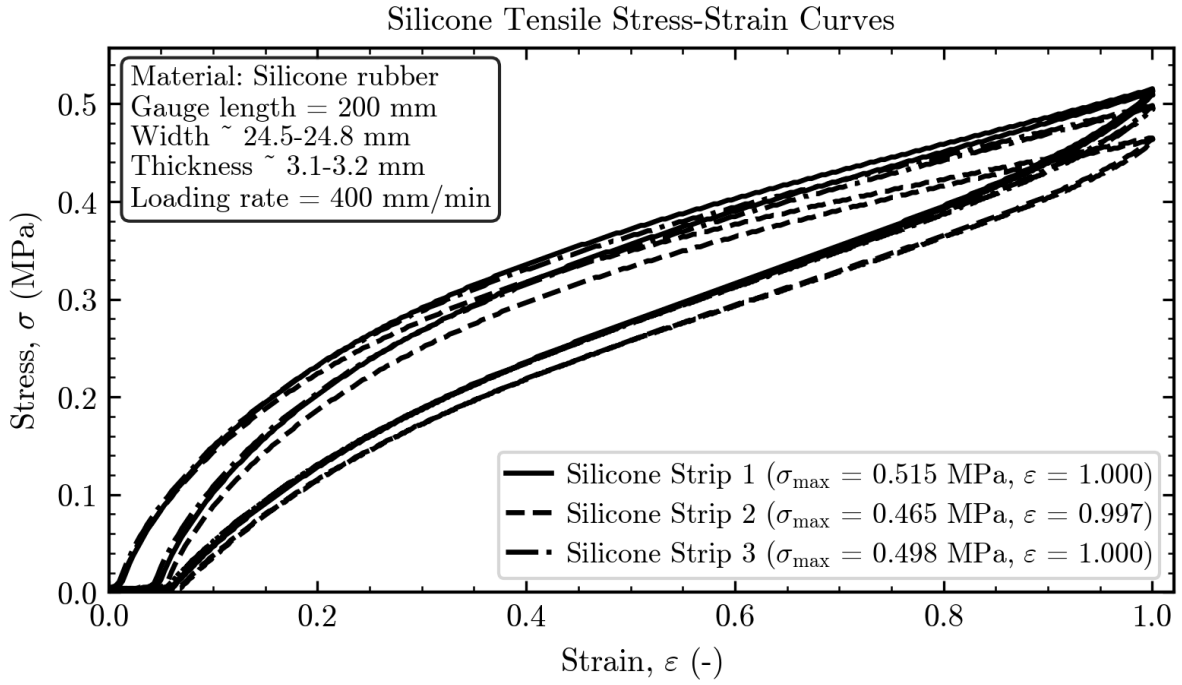

Figure 1: Engineering stress–strain curves for three silicone strip specimens subjected to uniaxial tension at 400 mm/min (gauge length 200 mm). All samples exhibited highly repeatable nonlinear elastic behavior with pronounced hysteresis between loading and unloading segments. Peak engineering stresses ranged from 0.465 to 0.515 MPa, with maximum strains of approximately 1.0.

3.3 Unconfined Compression Response of Porcine Muscle

The unconfined compression behavior of porcine skeletal muscle exhibited markedly different characteristics from that of silicone rubber, reflecting the intrinsic heterogeneity and anisotropy of biological soft tissue. The engineering stress–strain curves for the three muscle specimens are shown in Figure 3-5. All samples demonstrated nonlinear stiffening behavior with increasing axial strain, consistent with the expected response of hydrated, fiber-reinforced soft tissues under compression. However, notable specimen-to-specimen variability was observed, particularly in the smoothness and local fluctuations of the stress signals.

Sample 1 displayed continuous small-amplitude peaks superimposed on the rising stress–strain trend. This textured appearance arises from micro-scale structural rearrangements within the muscle, including fiber–fiber sliding, fascicle reorientation, and local stick–slip events at the platen–tissue interface. These microscopic redistributions of load produce high-frequency fluctuations that are characteristic of heterogeneous biological tissues. Despite these fluctuations, the overall slope of the curve remained comparable to the other specimens, indicating similar bulk stiffness.

Sample 2 exhibited a much smoother and more uniform stress–strain curve, with minimal high-frequency noise. This suggests a more homogeneous internal structure or more stable boundary contact during compression. The curve showed progressive stiffening up to a peak stress of approximately 28 kPa, followed by rapid unloading at the end of the test sequence.

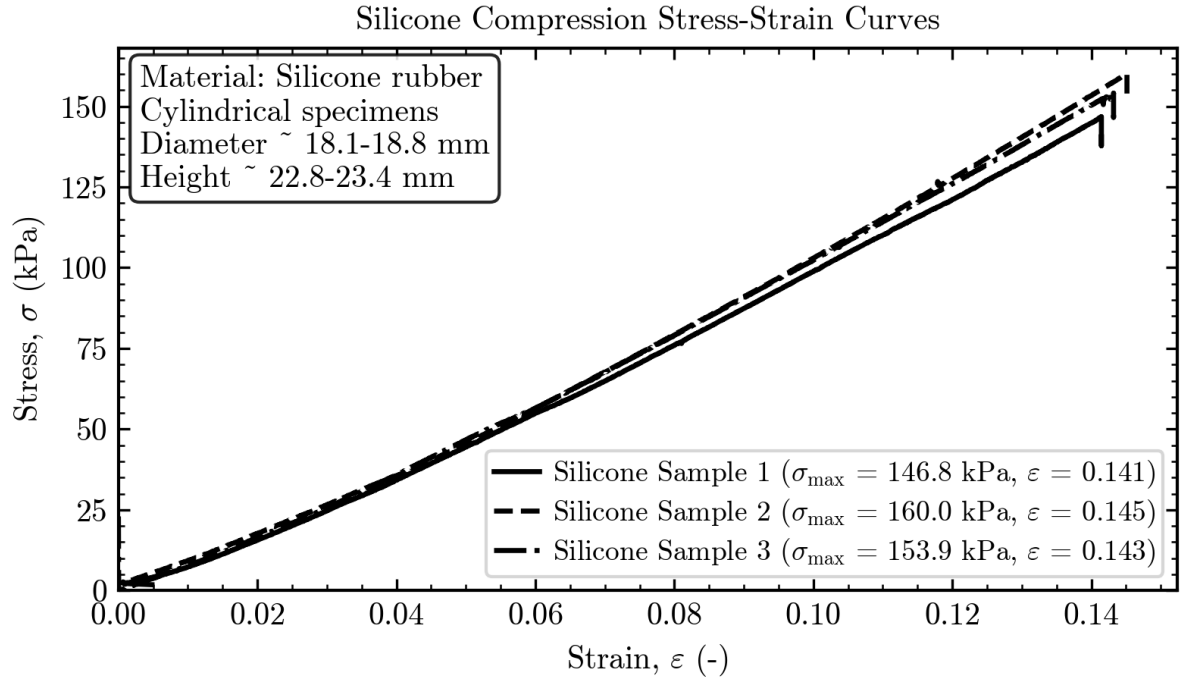

Figure 2: Engineering stress–strain curves for three cylindrical silicone specimens under unconfined compression. The samples displayed smooth, nonlinear stiffening behavior with minimal variability across specimens. Peak stresses ranged from 146 to 160 kPa, with maximum engineering strains of approximately 0.14.

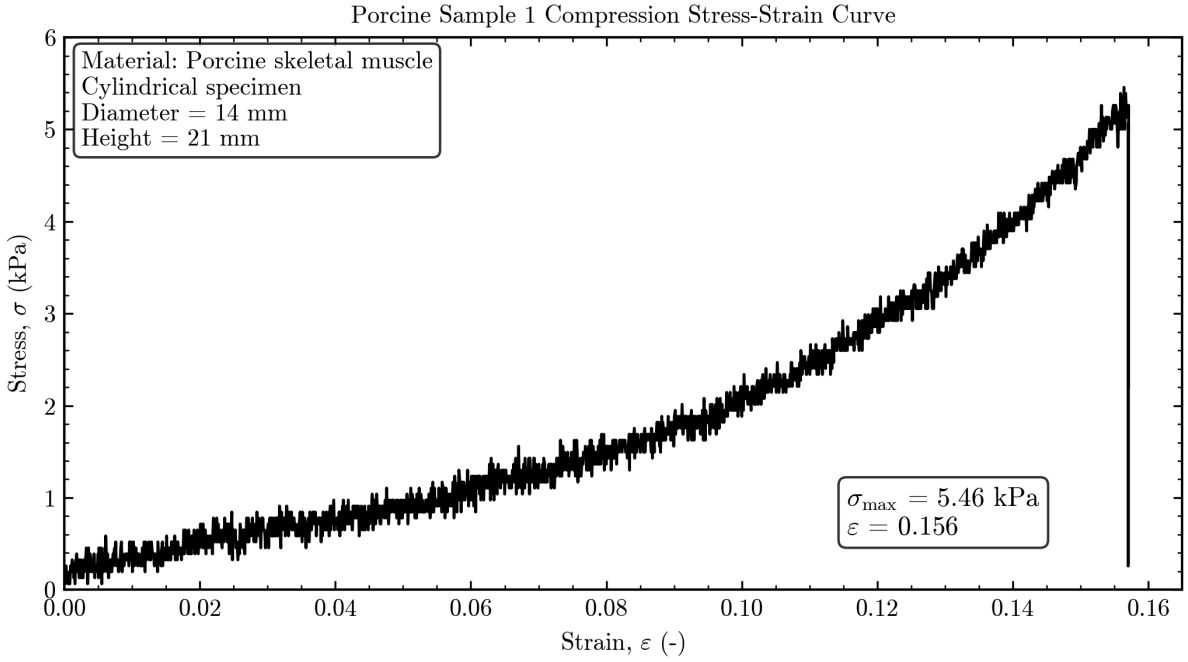

Figure 3: Engineering stress–strain response of Porcine Sample 1 during unconfined compression. The curve exhibits nonlinear stiffening accompanied by continuous small-amplitude fluctuations, characteristic of heterogeneous biological soft tissues. The maximum stress reached 5.46 kPa at an engineering strain of 0.156.

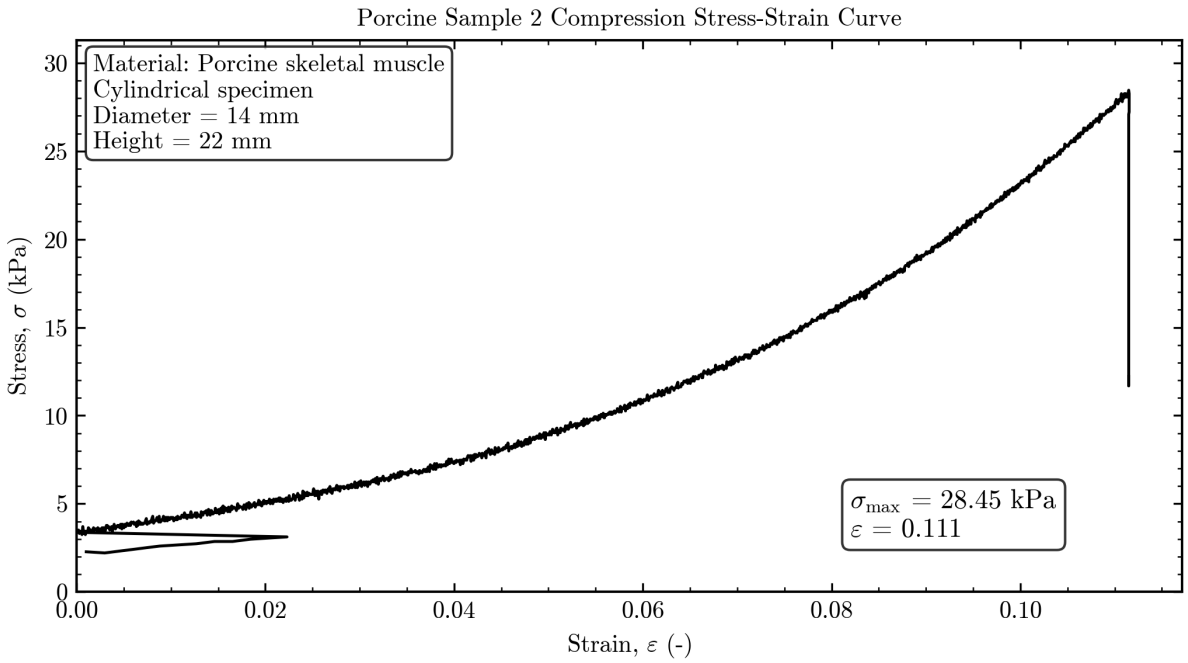

Figure 4: Engineering stress–strain response of Porcine Sample 2 during unconfined compression. This specimen demonstrated a smooth and uniform stress–strain profile with minimal high-frequency variability, reaching a peak stress of 28.45 kPa at an engineering strain of 0.111.

Sample 3, although smoother than Sample 1, contained several distinct localized spikes. These larger peaks likely reflect isolated structural discontinuities such as connective tissue bundles or small fat pockets that momentarily resisted deformation. The overall mechanical response was intermediate between Sample 1 and Sample 2, again emphasizing the natural variability present among biological specimens.

Despite these differences in curve texture, all three muscle samples exhibited similar nonlinear stiffening behavior, reinforcing the characteristic response of porcine skeletal muscle as a hydrated, viscoelastic, fiber-reinforced material. The combined results highlight that biological tissues, unlike synthetic elastomers, inherently possess microstructural irregularities that manifest as variability in the stress–strain signal, even when specimens have nearly identical dimensions and testing conditions.

3.4 Stress Relaxation Behavior of Compression

Stress relaxation behavior was characterized exclusively under uniaxial compression. Following the ramp phase, the maximum displacement (3.3 mm) was held constant for 120 seconds to observe the time-dependent stress decay. Note that tensile tests consisted of continuous load-unload cycles and did not include a relaxation hold phase.

Figure 6 displays the stress-time response for the three silicone specimens. The material exhibited minimal viscoelasticity, maintaining a relatively stable stress level during the hold period. The stress decreased from the peak value by approximately 4.5% over the 120-second duration. This limited relaxation confirms that the silicone acts primarily as a hyperelastic solid with negligible viscous dissipation under these loading conditions.

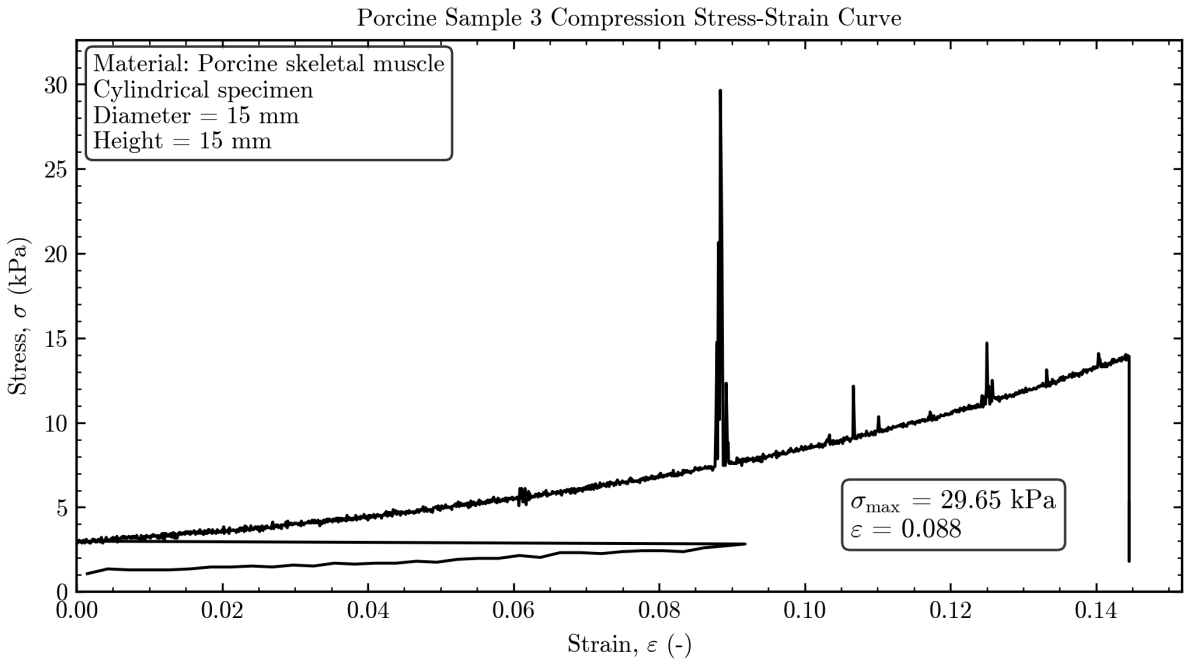

Figure 5: Engineering stress–strain response of Porcine Sample 3 during unconfined compression. The curve shows nonlinear stiffening with several discrete localized stress peaks, likely caused by structural heterogeneities within the tissue. The maximum stress recorded was 29.65 kPa at an engineering strain of 0.088.

In contrast, porcine muscle tissue demonstrated pronounced viscoelastic behavior, as shown in Figure 7. The stress decayed rapidly within the first few seconds of the hold phase, followed by a slower asymptotic decline. On average, the stress relaxed by approximately 58.7% from its peak value. The significant difference in relaxation magnitude between the three muscle specimens further highlights the biological heterogeneity of the tissue compared to the synthetic silicone.

3.5 Comparison of Tensile and Compressive Behavior

Figure 8 presents the combined Cauchy stress-stretch response of the silicone elastomer across both compressive ($\lambda < 1$) and tensile ($\lambda > 1$) regimes. The material exhibits a continuous transition through the undeformed state ($\lambda = 1, \sigma = 0$).The response reveals an asymmetry in stiffness dependent on the loading mode. In the small deformation range ($0.85 < \lambda < 1.15$), the slope of the curve (tangent modulus) is continuous. However, as deformation increases, the tensile response exhibits pronounced strain-stiffening (upward curvature), whereas the compressive response remains relatively linear. Quantitatively, the initial modulus calculated from compression ($\mu \approx 0.45$ MPa) is consistent with the shear modulus components derived from the large-strain tensile fit (Table 1), confirming the material's isotropic nature.

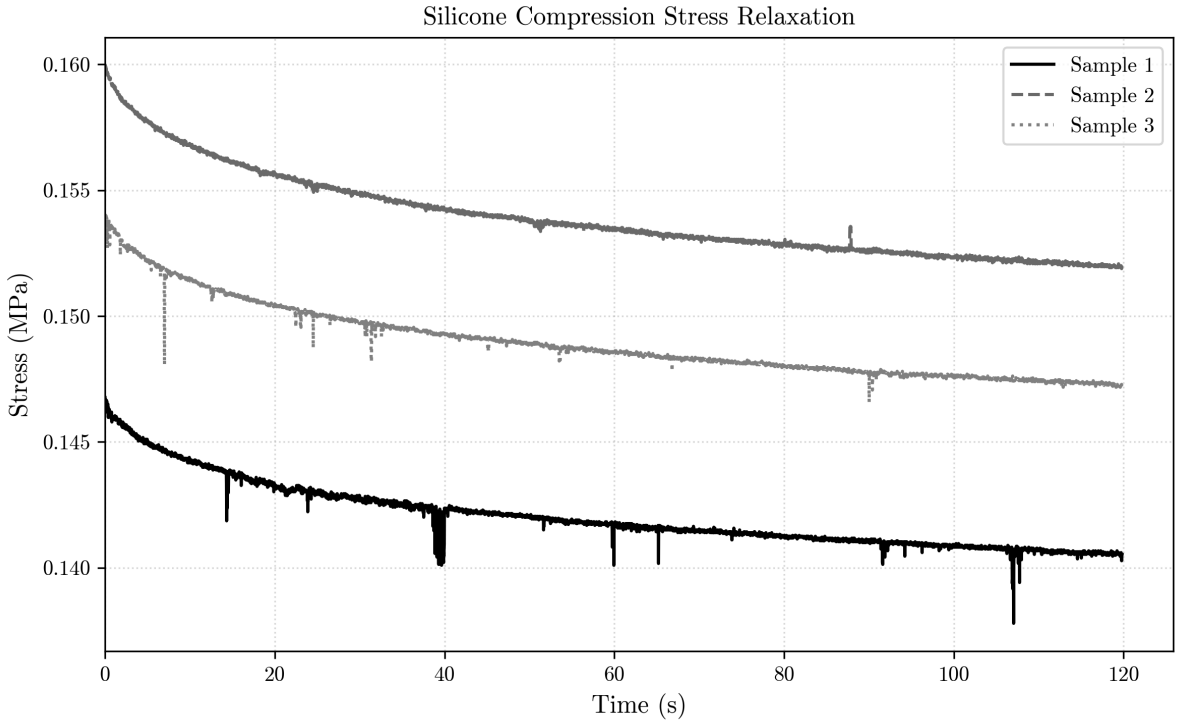

Figure 6: Stress relaxation response of silicone elastomer under uniaxial compression (holding at 3.3 mm displacement). The stress exhibits a minimal decay of approximately 4.5% over 120 seconds, indicating predominantly elastic behavior.

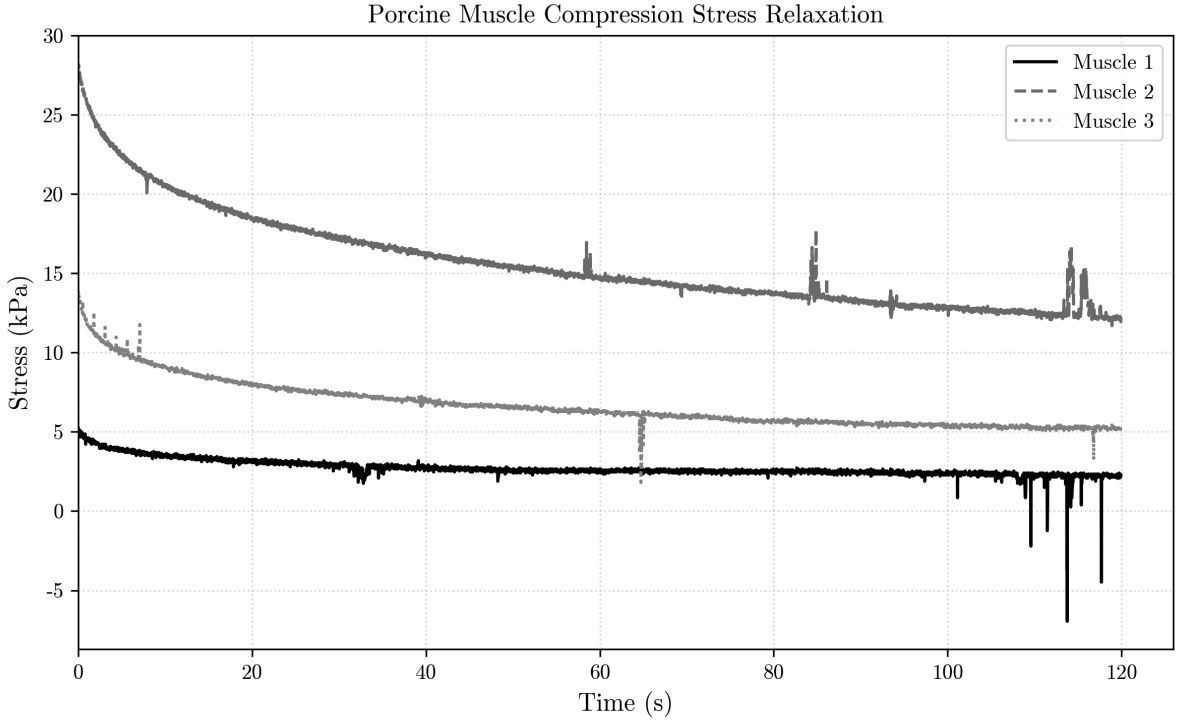

Figure 7: Stress relaxation response of porcine skeletal muscle under uniaxial compression. The tissue exhibits strong viscoelasticity, with an average stress decay of approximately 58.7% over the 120-second hold period. The variation between curves reflects the structural heterogeneity of the biological samples.

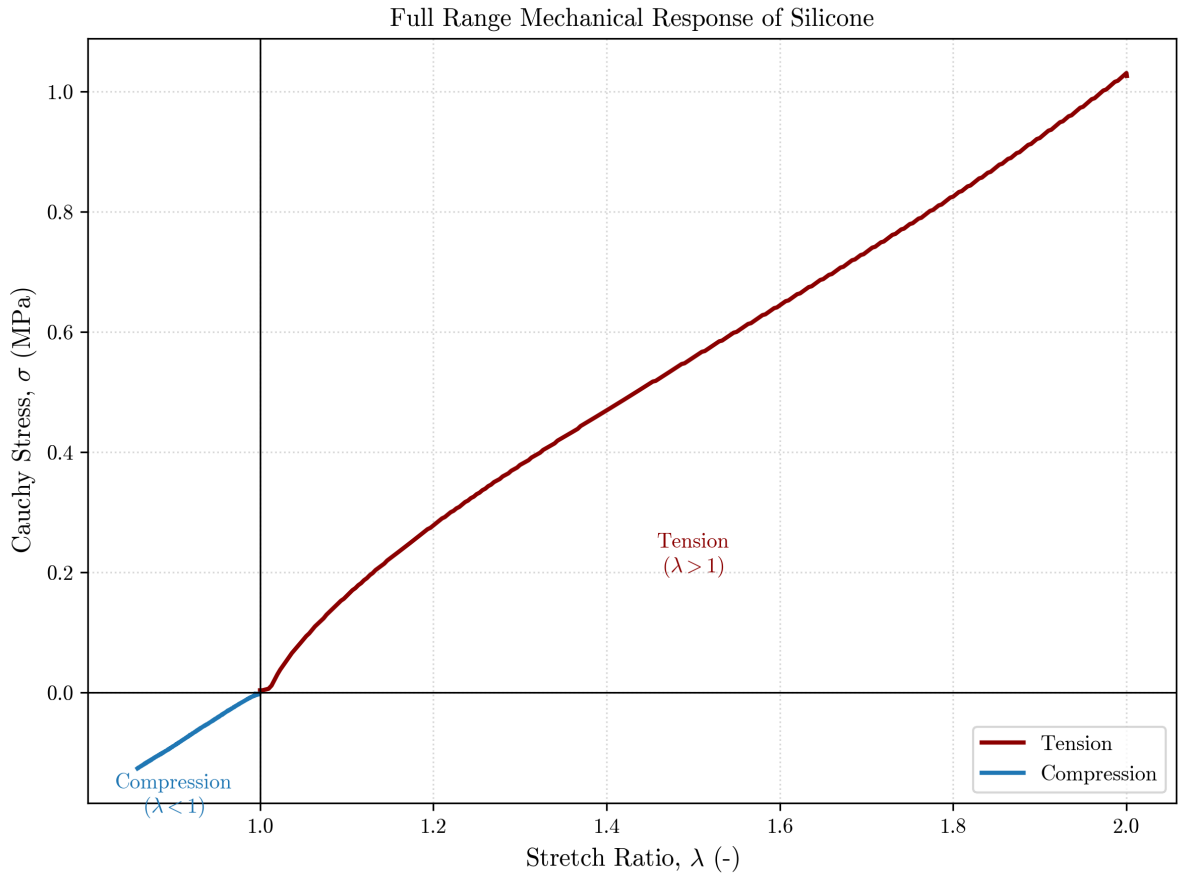

Figure 8: Full-range mechanical response of silicone elastomer showing engineering stress versus stretch ratio. The curve combines uniaxial compression data (blue, $\lambda < 1$) and uniaxial tension data (red, $\lambda > 1$). The continuity at $\lambda = 1$ and the consistency in initial stiffness indicate isotropic material behavior, while the large-strain tension data reveals significant strain-stiffening.

3.6 Ogden Hyperelastic Model Fitting

The first loading segment of each silicone tensile curve was fitted using an incompressible four-term Ogden hyperelastic model (N = 4). The fitted parameters (Table 1) reproduced the experimental stress–stretch response with high fidelity, as shown in Figure 9. The multi-term model accurately captured the pronounced strain stiffening at large stretches and yielded a global goodness-of-fit of $R^2 \approx 0.997$ ($SSE \approx 0.345$). Minor deviations at the highest stretches are attributable to viscoelasticity, which is not included in the purely elastic Ogden formulation.

For silicone compression, the deformation range was small (engineering strains < 0.15, $\lambda \gtrsim 0.85$). The stress–stretch response was therefore fitted using a one-term Ogden model (N = 1). As shown in Figure 10, the one-term model provided an excellent match to all three specimens, yielding parameters $\mu \approx 0.335$ MPa and $\alpha \approx 13.41$, with $R^2 \approx 0.996$. These results confirm that silicone behaves as a consistent, nearly isotropic hyperelastic material even in mild compression.

Porcine muscle was also fitted using a one-term Ogden model (N = 1). Due to the tissue's inherent heterogeneity, the experimental curves exhibited substantial inter-specimen variability, particularly in localized stress fluctuations. A global Ogden fit across all samples (Figure 11) yielded $\mu \approx 23.73$ kPa and a nonlinearity parameter $\alpha \approx -1.26$, with a lower coefficient of determination ($R^2 \approx 0.448$) reflecting the biological variability. The results highlight the much lower stiffness of muscle compared to silicone, as well as its heterogeneous internal structure and strong time-dependent behavior.

Table 1: Fitted material parameters for the four-term incompressible Ogden hyperelastic model. The model was fitted to the uniaxial tensile loading data of three silicone specimens.

Parameter (i)	**Shear Modulus μ_i (MPa)**	**Exponent α_i (-)**
1	0.2407	-6.419
2	0.1260	1.702
3	0.2291	-6.419
4	0.0639	1.703
SSE = 0.3452	$R^2 = 0.9965$	

3.7 Summary of Experimental Observations

Representative photographs of the testing configurations are presented in Figure 12(a) (Silicone Tension), Figure 12(b) (Silicone Compression), and Figure 12(c) (Porcine Muscle Compression). These visual observations corroborate the quantitative mechanical characterization: **Tensile Behavior.** The silicone strips exhibited uniform deformation under large strains (as shown in Figure 12(a)). This geometric consistency aligns with the high fidelity of the four-term Ogden model fit ($R^2 = 0.997$) and confirms the material's nature as an isotropic, hyperelastic solid.

Material Contrast. A visual comparison between the synthetic silicone (Figure 12(b))

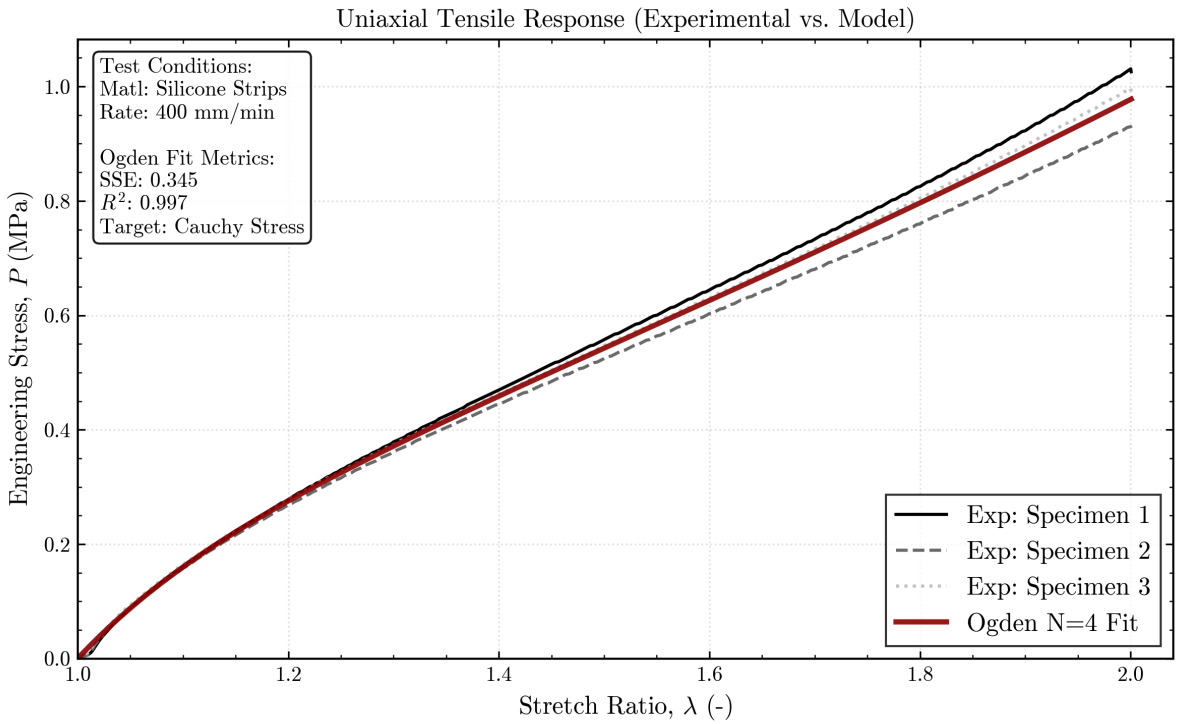

Figure 9: Uniaxial tensile Engineering stress–stretch response of silicone elastomer strips. Experimental curves from three specimens are shown alongside the fitted Ogden hyperelastic model (N = 4).

and the biological tissue (Figure 12(c)) highlights distinct structural differences. The silicone retained a regular cylindrical shape, corresponding to its linear, stiff compressive response ($\mu \approx 0.335$ MPa). In contrast, the porcine muscle appeared irregular and heterogeneous, which explains the high inter-specimen variability and significantly lower stiffness ($\mu \approx 23.73$ kPa) observed in the data.

Viscoelasticity. The silicone demonstrated minimal stress relaxation (∼4.5%), consistent with its stable solid appearance. Conversely, the porcine muscle showed significant viscoelastic decay (∼58.7%), characteristic of fluid-filled biological tissues.

Tension–Compression Asymmetry. The full-range response curve (Figure 8) illustrates that while silicone behaves linearly in compression (small deformation), it exhibits substantial strain-stiffening in tension (large deformation), necessitating different modeling approaches ($N = 1$ vs. $N = 4$) depending on the loading mode.

4 Discussion

4.1 Hyperelastic Constitutive Modeling: Applicability and Limitations

The four-term Ogden model reproduced the tensile loading curve of silicone with high fidelity ($R^2 = 0.997$), confirming that the material behaves as an incompressible hyperelastic solid under large principal stretch. However, a notable limitation of this approach

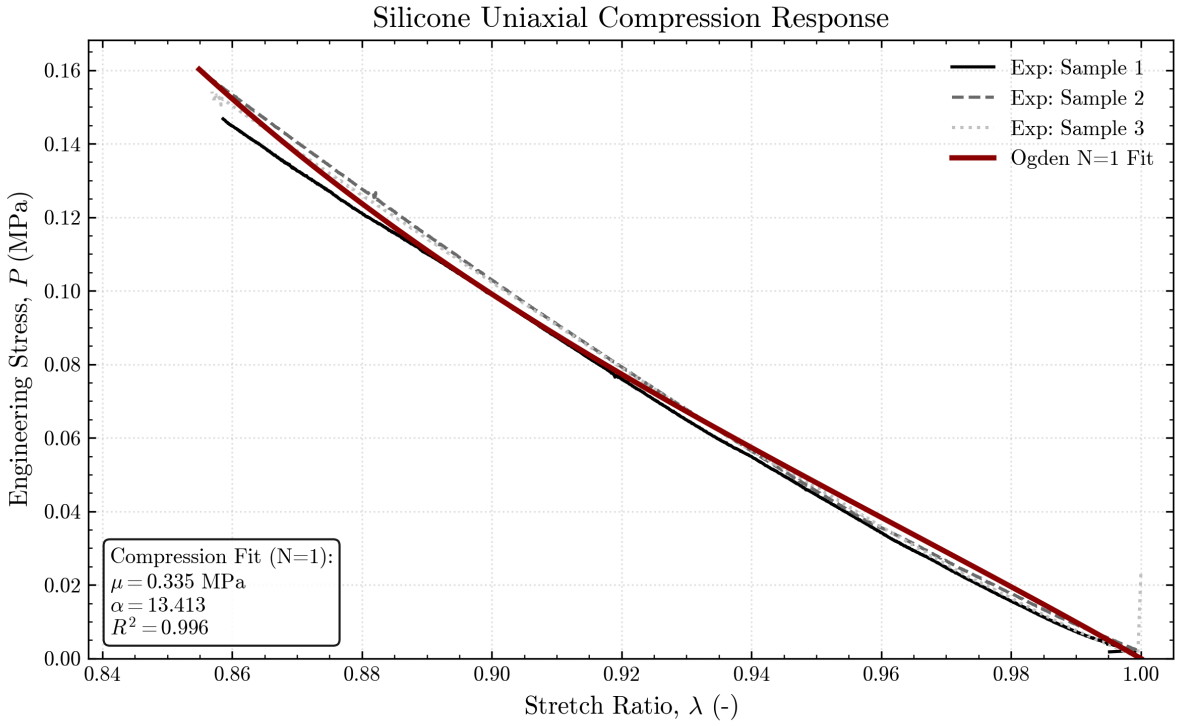

Figure 10: Uniaxial compressive stress-stretch behavior of silicone elastomer compared with a one-term ($N = 1$) Ogden hyperelastic model fit. Experimental data (black/gray lines) show the response of three cylindrical specimens compressed at 5 mm/min. The solid red curve represents the best-fit model, plotting the compressive stress magnitude P versus stretch λ. Fitted material constants (μ, α) and the coefficient of determination (R^2) are displayed in the inset.

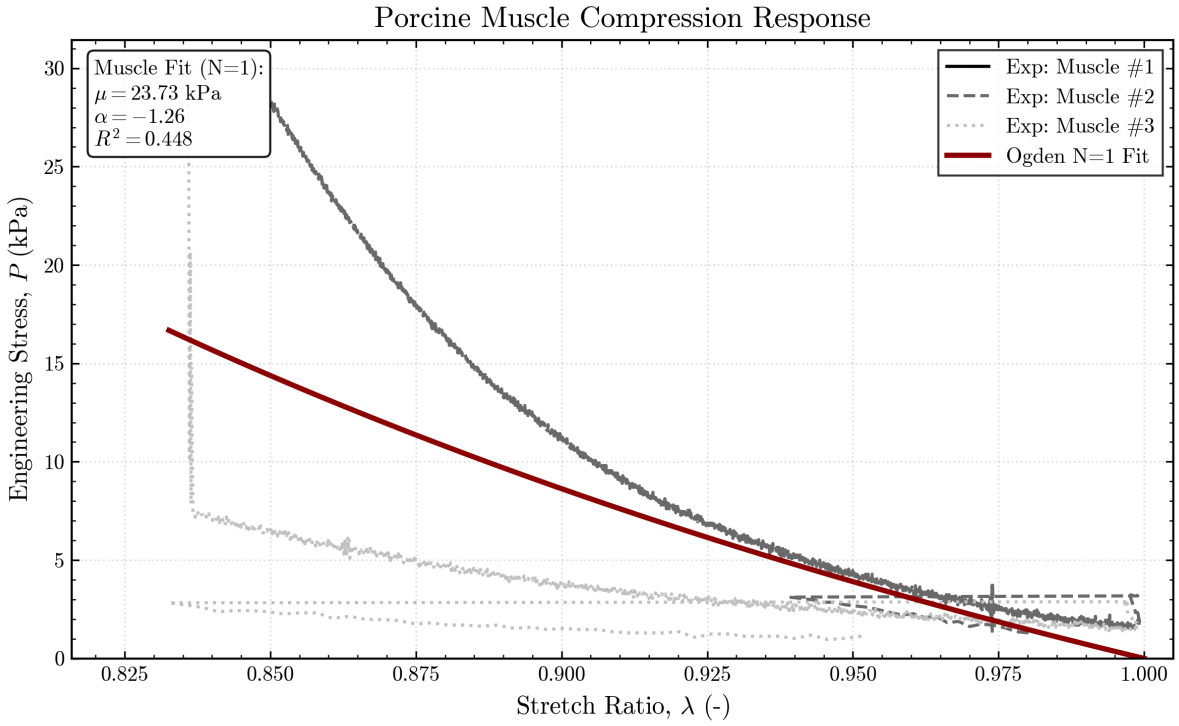

Figure 11: Uniaxial compressive stress-stretch behavior of porcine skeletal muscle (n=3) and the corresponding Ogden ($N = 1$) model fit. The significant variation between specimens (black/gray curves) highlights the heterogeneity inherent in biological tissue. The global fit (red line) yields shear modulus $\mu = 23.7293$ kPa and non-linearity parameter $\alpha = -1.2611$. Note the stress scale in kPa, indicating significantly lower stiffness compared to silicone.

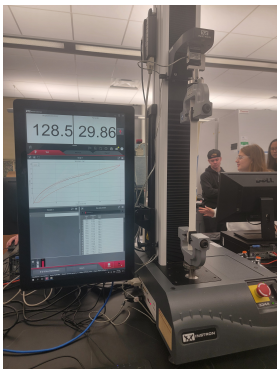

(a) Silicone Uniaxial Tension Setup

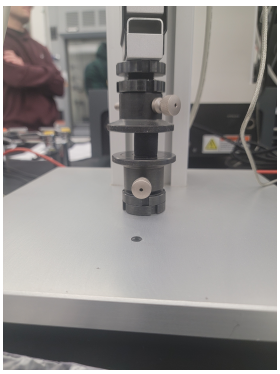

(b) Silicone Compression Setup

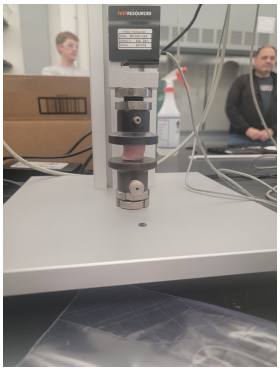

(c) Porcine Muscle Compression Setup

Figure 12: Visual summary of experimental setups. (a) Silicone strip undergoing uniaxial tension. (b) Cylindrical silicone specimen showing regular geometry. (c) Porcine skeletal muscle specimen highlighting biological heterogeneity.

is that the Ogden formulation is purely elastic: it contains no viscous or time-dependent terms. The pronounced hysteresis observed in the tensile load–unload cycle (Figure 1) and the finite stress relaxation under compression (Figure 6) both indicate that silicone possesses non-negligible viscoelastic character, even if mild ($\sim$4.5% relaxation). Fitting only the first loading segment, as done here, therefore captures the quasi-static elastic response while systematically excluding energy dissipation. A more complete constitutive description would employ a finite-strain viscoelastic framework, such as a quasi-linear viscoelasticity (QLV) formulation or a multiplicative decomposition of the deformation gradient into elastic and viscous parts [1]. Within the scope of this study, however, the purely elastic Ogden model is a well-justified approximation for characterizing the dominant stiffness response of silicone.

The one-term Ogden fit for silicone compression ($\mu \approx 0.335$ MPa, $\alpha \approx 13.41$, $R^2 = 0.996$) is consistent with the dominant shear modulus recovered from the tensile fit. The large exponent $\alpha \approx 13$ reflects that the material stiffens rapidly with strain even in the mild compression regime tested here ($\lambda \gtrsim 0.85$). Taken together, the compressive and tensile fits support the isotropic, near-incompressible characterization of the silicone used in this study, which is consistent with typical room-temperature silicone elastomers reported in the literature (shear moduli in the range 0.1–1 MPa depending on crosslink density).

For porcine skeletal muscle, the global one-term Ogden fit yielded a poor coefficient of determination ($R^2 \approx 0.448$), reflecting substantial inter-specimen variability rather than an inadequacy of the Ogden functional form per se. The fitted shear modulus ($\mu \approx 23.73$ kPa) and negative nonlinearity exponent ($\alpha \approx -1.26$) are broadly consistent with reported values for passive skeletal muscle under unconfined compression in the literature, which typically fall in the range 1–50 kPa depending on fiber orientation, hydration state, and postmortem condition. The negative α value indicates an initial softening followed by rehardening, which can arise from interstitial fluid redistribution and fiber reorientation at low strains — a behaviour distinct from rubber-like strain stiffening. A fiber-reinforced or transversely isotropic constitutive model would more accurately represent muscle's directional microstructure, but is beyond the scope of this introductory characterization.

4.2 Sources of Experimental Variability

The silicone specimens demonstrated high repeatability across both tensile and compressive tests, consistent with the controlled fabrication process of synthetic elastomers. Residual variation between specimens in the tensile curves (Figure 1) most likely reflects minor differences in specimen geometry, grip alignment, or slight pre-stretch introduced during clamping. These effects are expected to be small given the low initial compliance of silicone.

In contrast, the porcine muscle specimens showed substantial inter-specimen variability in both curve texture and peak stress magnitude. Three distinct mechanisms are responsible. First, biological heterogeneity: skeletal muscle is composed of fiber bundles, connective tissue (perimysium, epimysium), and adipose inclusions, whose spatial distribution varies between samples even from the same muscle group. Second, anisotropy: the cylindrical specimens were not consistently oriented with respect to fiber direction, meaning some samples were compressed along the fiber axis and others transversely, producing inherently different mechanical responses. Third, postmortem degradation: porcine tissue undergoes

progressive stiffness changes after death due to ATP depletion and rigor mortis onset; any variability in the time between slaughter and testing would contribute to scatter in the data.

These sources of variability highlight a fundamental challenge in soft tissue biomechanics: meaningful constitutive characterization requires either a much larger sample cohort to perform statistical averaging, or careful specimen-specific protocols that control fiber orientation and standardize testing timelines.

4.3 Tension–Compression Asymmetry and Modelling Implications

The full-range stress–stretch response (Figure 8) reveals a clear asymmetry between the tensile and compressive regimes: the material behaves in an approximately linear fashion under mild compression ($\lambda \gtrsim 0.85$), yet exhibits pronounced strain stiffening under tension at $\lambda \approx 2$. This asymmetry is a well-known feature of rubber-like materials and arises from the underlying network statistics of polymer chains. At small compressive strains the affine network is barely perturbed, whereas at large tensile strains chains approach their extensibility limit, causing the rapid stiffness upturn captured by the Ogden model.

From a modelling standpoint, this asymmetry justifies using different levels of model complexity for the two regimes: a one-term Ogden model is sufficient in mild compression, while four terms are required to faithfully represent the full tensile nonlinearity. It also implies that material parameters obtained from a purely compressive experiment cannot be directly extrapolated to predict large-strain tensile behavior, and vice versa. For applications such as soft robotic actuators or surgical simulation, where both loading modes are present, a single multi-term model fitted to combined tension–compression data would be preferable.

4.4 Broader Relevance to Soft Tissue Analogues

The comparison between silicone and porcine muscle is directly relevant to the design of tissue-mimicking phantoms for biomechanical testing and medical device validation. The order-of-magnitude difference in shear modulus (silicone $\sim$0.335 MPa vs. muscle $\sim$23.7 kPa) confirms that unmodified silicone elastomers are too stiff to replicate the passive mechanical response of skeletal muscle. Achieving a better match would require either the use of softer silicone formulations (higher oil-to-crosslinker ratio) or alternative hydrogel-based materials such as polyvinyl alcohol or gelatin, which can be tuned to the kPa stiffness range. Furthermore, the strongly viscoelastic nature of muscle ($\sim$58.7% stress relaxation) suggests that any credible tissue phantom must incorporate time-dependent constitutive behavior, a requirement that purely elastic silicone cannot satisfy.

5 Conclusions

Based on the experimental results and constitutive modeling, the following conclusions are drawn: **Hyperelastic Modeling Accuracy.** The four-term incompressible Ogden

model ($N = 4$) successfully captured the nonlinear strain-stiffening behavior of silicone rubber under large tensile deformation ($\lambda = 2.0$). The global fit demonstrated excellent fidelity to the experimental stress data, yielding a coefficient of determination of $R^2 = 0.997$ and a low sum of squared errors (SSE = 0.345).

Stiffness Comparison. Silicone exhibited a compressive shear modulus of approximately $\mu \approx 0.335$ MPa, whereas the porcine skeletal muscle was significantly more compliant with a modulus of $\mu \approx 23.73$ kPa. This indicates that the synthetic elastomer is approximately 14 times stiffer than the biological tissue tested.

Viscoelastic Behavior. The two materials demonstrated distinct time-dependent responses. Silicone behaved as a predominantly elastic solid with minimal stress relaxation ($\sim$4.5% decay over 120 seconds). In contrast, porcine muscle exhibited strong viscoelasticity, with stress relaxing by approximately $\sim$58.7% over the same duration, reflecting the fluid-filled, porous nature of biological tissue.

Material Homogeneity. The silicone specimens showed high repeatability and consistent stiffness across tensile and compressive modes, confirming isotropic behavior. Conversely, the porcine muscle samples displayed high inter-specimen variability ($R^2 \approx 0.448$ for the global fit), highlighting the inherent structural heterogeneity of biological soft tissues.

References

[1] R. W. Ogden. Large deformation isotropic elasticity: On the correlation of theory and experiment for incompressible rubberlike solids. *Proceedings of the Royal Society of London. Series A*, 1972.